JBC RESEARCH ARTICLE

m6A demethylation of cytidine deaminase *APOBEC3B* mRNA orchestrates arsenic-induced mutagenesis

Received for publication, October 4, 2021, and in revised form, December 28, 2021 Published, Papers in Press, January 6, 2022,
https://doi.org/10.1016/j.jbc.2022.101563

Ming Gao[1,2,‡], Zijuan Qi[3,‡], Wenya Feng[1,2], Hongyang Huang[4], Zhijie Xu[5], Zheng Dong[1,2], Ming Xu[1,2], Jinxiang Han[3], Jake A. Kloeber[6,7], Jinzhou Huang[6,*], Zhenkun Lou[6,*], and Sijin Liu[1,2,*]

From the [1]State Key Laboratory of Environmental Chemistry and Ecotoxicology, Research Center for Eco-Environmental Sciences, Chinese Academy of Sciences, Beijing, China; [2]College of Resources and Environment, University of Chinese Academy of Sciences, Beijing, China; [3]Department of Orthopedic Surgery, The First Affiliated Hospital of Shandong First Medical University, Ji'nan, Shandong, China; [4]Department of Pathology, Li Ka Shing Faculty of Medicine, The University of Hong Kong, Hong Kong, China; [5]Department of Pathology, National Clinical Research Center for Geriatric Disorders, Xiangya Hospital, Central South University, Changsha, Hunan, China; [6]Department of Oncology, and [7]Mayo Clinic Medical Scientist Training Program, Mayo Clinic, Rochester, Minnesota, USA

Edited by Eric Fearon

The cytidine deaminase APOBEC3B (A3B) is an endogenous inducer of somatic mutations and causes chromosomal instability by converting cytosine to uracil in single-stranded DNA. Therefore, identification of factors and mechanisms that mediate A3B expression will be helpful for developing therapeutic approaches to decrease DNA mutagenesis. Arsenic (As) is one well-known mutagen and carcinogen, but the mechanisms by which it induces mutations have not been fully elucidated. Herein, we show that A3B is upregulated and required for As-induced DNA damage and mutagenesis. We found that As treatment causes a decrease of N6-methyladenosine (m6A) modification near the stop codon of A3B, consequently increasing the stability of A3B mRNA. We further reveal that the demethylase FTO is responsible for As-reduced m6A modification of A3B, leading to increased A3B expression and DNA mutation rates in a manner dependent on the m6A reader YTHDF2. Our *in vivo* data also confirm that A3B is a downstream target of FTO in As-exposed lung tissues. In addition, FTO protein is highly expressed and positively correlates with the protein levels of A3B in tumor samples from human non–small cell lung cancer patients. These findings indicate a previously unrecognized role of A3B in As-triggered somatic mutation and might open new avenues to reduce DNA mutagenesis by targeting the FTO/m6A axis.

Somatic mutations are the predominant cause for the malignant transformation of various cancers (1, 2). DNA deaminase APOBEC family members, especially APOBEC3B (A3B), have been considered as endogenous drivers of mutations (3). There are seven APOBEC3 family members (APOBEC3A/B/C/D/F/G/H) in humans and only one (APOBEC3) in mice. A3B overexpression correlates with signature C to T mutations, base substitution mutation loads dispersed throughout the genome, and clustered regions of hypermutation (kataegis) in multiple types of cancer including breast and lung cancers (4–7). A3B is predominantly located in the nucleus, and its overexpression can trigger strong DNA damage responses, exacerbate DNA replication stress and chromosomal instability, or cause cell cycle arrest and cell death (8, 9). A few explanations have been made to answer how A3B expression and activity are regulated. For example, oncogenic signaling and chemotherapy drugs modulate the activity of A3B by increasing the availability of ssDNA substrate (10–12); transcriptional regulators such as c-Maf, B-Myb, ZNF384, and oncogenic NF-κB signaling are involved in A3B transcription and promote C-to-T transitions in multiple cancer types (13–16); MSL2 activates hepatitis B virus replication and maintains hepatitis B virus covalently closed circular DNA stability through the degradation of A3B protein to enhance hepatocellular carcinoma progression (17). However, there are currently no available drugs to reduce A3B levels and thus limit mutagenesis.

N6-methyladenosine (m6A) is the most prevalent internal modification of RNA molecules that occurs at the consensus motif, RRACH (R is G or A or U and H is U, A, or C) (18, 19). It can reversely influence various biological processes by affecting mRNA translation, mRNA degradation, pre-mRNA splicing, and protein–RNA interactions (18, 19). The deposition of m6A modification is catalyzed by its writer, the m6A methyltransferase complex which composed of METTL3, METTL14, and WTAP, and the removal of m6A is mainly driven by demethylase erasers (FTO and ALKBH5). The m6A modification can be recognized by its readers (Ythdf and Ythdc families) which determine the fate of target RNAs (18, 19). Among these m6A modulators, FTO is the first identified m6A demethylase that mediates m6A demethylation in the 3′-UTR and near stop codon region (20). FTO participates in diverse physiological and pathological processes, notably it plays an oncogenic role in a variety of cancers (21, 22). It is reported that alteration of FTO expression is involved in metabolic starvation stress, acute liver injury, or heart failure (23–25).

‡ These authors contribute equally to this work.
* For correspondence: Zhenkun Lou, lou.zhenkun@mayo.edu; Sijin Liu, sjliu@rcees.ac.cn; Jinzhou Huang, huang.jinzhou@mayo.edu.

GSK3-mediated FTO phosphorylation and degradation regulates the pluripotency of mouse embryonic stem cells (26). However, until now, the regulatory mechanisms and downstream targets of FTO are still largely unknown.

Arsenic (As) is a highly toxic carcinogen and widespread in the environment. Many epidemiologic studies have established the association between the occurrence of cancers and chronic exposure to high levels of As (27, 28). It is reported that As triggers the DNA damage response and interferes with DNA repair by indirectly generating oxidative stress (29). However, the precise mechanisms of As-induced mutagenesis remain ill-defined and under debate. Here, we found that As treatment enhanced the somatic mutation rate by increasing A3B expression level. Further analysis showed that FTO was upregulated and responsible for As-induced A3B expression in an m6A-dependent manner. FTO removed the m6A modification from a consensus m6A motif near the stop codon of A3B, decreasing the decay of A3B mRNA by YTHDF2, which led to increased A3B level and DNA mutagenesis in As-treated cells. In addition, As exposure also induced an increase of A3B in the lung tissues of mice in an FTO-dependent manner. Moreover, A3B is overexpressed in the tumor tissue of lung cancer patients and positively correlates with FTO levels. Together, these results depict a critical role of m6A methylation machinery in regulating As-induced somatic mutation.

Results

A3B induction accelerates As-induced mutagenesis

Previous studies showed that A3B induction by oncogene-induced replication stress or chemotherapy drugs enhances DNA editing and somatic mutations (30, 31). To investigate whether A3B expression was also responsible for As-induced mutagenesis, we first analyzed the expression level of A3B after low dose of As exposure. As shown in Fig. S1, *A* and *B*, the mRNA and protein levels of A3B were all increased after As treatment. Meanwhile, the mRNA levels of other APOBEC3 family members were not changed (Fig. S1*C*), indicating that A3B is an As-responsive gene and might play a critical role in As-induced mutagenicity and genotoxicity. We then used an *in vitro* cytosine deaminase assay and differential DNA denaturation PCR (3D-PCR) to detect whether As affects the enzymatic activity and mutagenic ability of A3B in control and A3B knockdown cells. As shown in Figure 1, *A*–*C*, As treatment enhanced cytidine deaminase activity in lysates from control cells but not in those from cells expressing A3B shRNA. In addition, the percentage of TP53 with higher A/T content that could be efficiently amplified at lower denaturation temperatures was increased after As treatment, and this mutation rate was attenuated in A3B-depleted cells (Fig. 1, *D* and *E*), indicating that As exposure induces the accumulation of nucleotide mutations by regulating the expression and enzymatic activity of A3B. Thereafter, we cloned and sequenced these 3D-PCR products to quantify the number and type of nucleotide mutations. As shown in Fig. S1*D* and Figure 1*F*, the percentage of amplicons with more than two nucleotide mutations was higher in As-treated cells than those in untreated cells, whereas the mutation rate declined to the normal level in A3B knockdown cells. In addition, the C/G to T/A transitions and transversions were the most prominent mutation types induced by As exposure (Fig. 1*G*). Taken together, these results demonstrate that A3B is likely the key mediator of As-driven somatic DNA mutation.

It was reported that A3B triggers DNA damage responses and cell death in UNG-knockout cells in p53-dependent manner (8); thus, we hypothesized that A3B expression is also required for As-induced genotoxicity and cytotoxicity in UNG-depleted cells. As shown in Fig. S1*E*, As exposure induced a significant increase of p53 expression in UNG-depleted cells. This appears to partly depend on A3B expression, because A3B depletion decreased the induction of p53 protein in these cells. Meanwhile, both the phosphorylation of ATM and CHK2 as well as γ-H2AX foci formation were significantly increased in control cells but not in A3B-depleted cells after As exposure (Fig. S1, *E*–*G*). In addition, the percentage of comet tail, an indicator of DNA damage, is much lower in A3B knockdown cells compared to that of control cells upon As treatment (Fig. S1, *H* and *I*), and these data indicate that A3B is a critical mediator for As-induced DNA damage. Moreover, As-reduced cell viability was also partly reversed by A3B depletion (Fig. S1, *J* and *K*), indicating that A3B induction is also involved in As-triggered cell death effects.

As regulates A3B expression through decreasing its m6A level

To determine how A3B mRNA level is regulated upon As treatment, we detected whether As treatment affects the mRNA stability of A3B. As shown in Figure 2*A*, A3B mRNA degraded much slower in As-treated cells than that in untreated cells after actinomycin D (ActD) treatment, suggesting that As treatment promotes the mRNA stability of A3B. Because m6A modification is critical for the regulation of mRNA stability, we analyzed the potential m6A sites in the mRNA of A3B through the website of SRAMP (http://www.cuilab.cn/sramp) and found that there are four conserved putative m6A consensus sequence GGAC (RRACH) motifs in the CDS region of A3B, and thus we inferred that m6A modification might be required for As-induced A3B expression. To confirm this hypothesis, we performed an RNA immunoprecipitation (RIP) assay to test whether an m6A-specific antibody recognizes A3B mRNA and found that A3B mRNA was strongly enriched after anti-m6A pull down (Fig. 2*B*). We next measured the total cellular m6A levels before and after As exposure. As shown in Figure 2, *C* and *D*, As treatment significantly decreased global m6A level by m6A dot blot assays and m6A colorimetric analysis, suggesting that m6A methylation is sensitive to As exposure. Gene-specific m6A quantitative real-time PCR (qPCR) assay was performed to further study whether As treatment affects the m6A modification of A3B. As shown in Figure 2*E*, As exposure decreased the m6A level of the A3B transcript, suggesting that A3B is a potential target of m6A modification.

To explore the role of m6A modification on the A3B transcript, four putative m6A consensus motifs on the CDS region of A3B were individually replaced from cytosine to thymine to

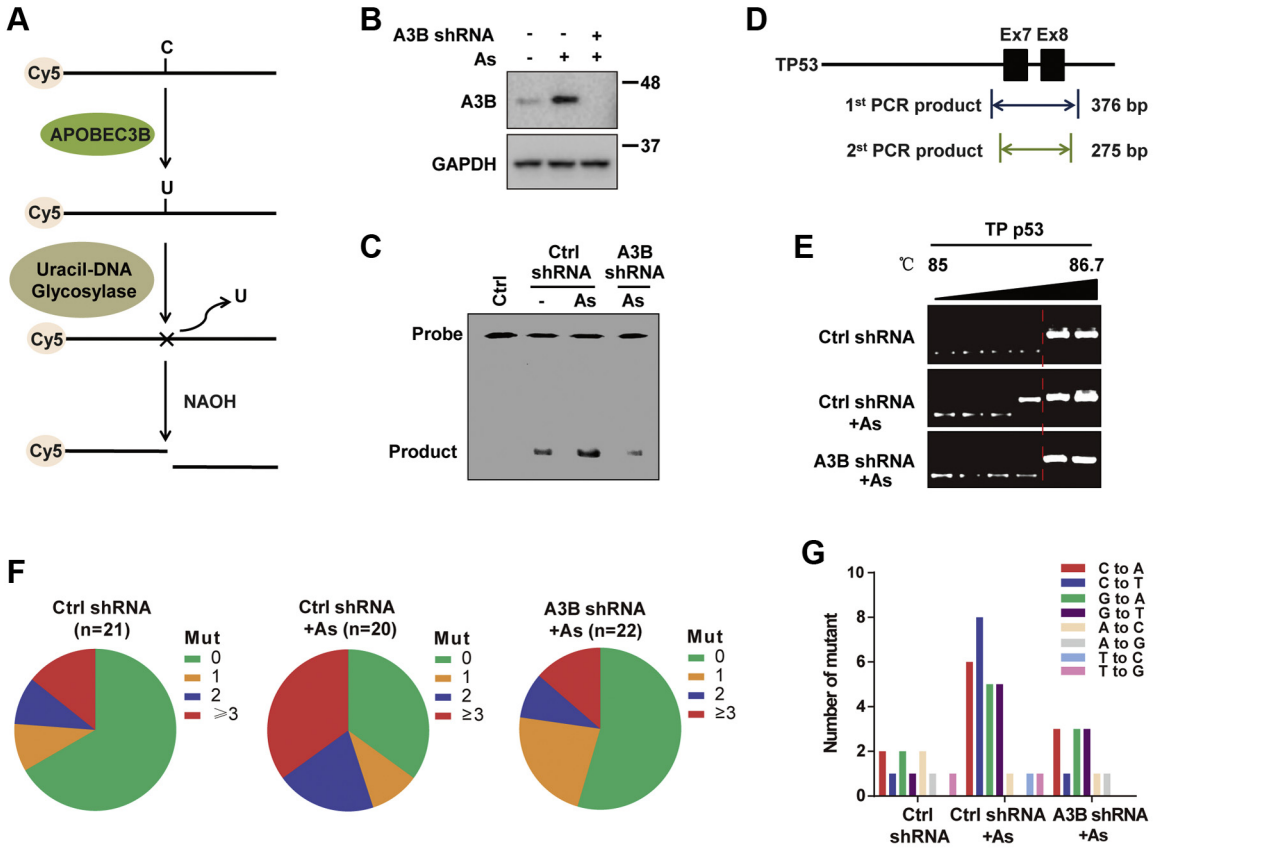

Figure 1. Arsenic treatment increases the protein level of A3B and exacerbates DNA mutation rates. *A*, illustration of the fluorescence-based DNA cytosine deamination assay. The ssDNA has a target cytosine, and Cy5-fluorescent, deaminase, and UDG enzyme create an abasic site and then broken by NAOH treatment. *B*, control or A3B-depleted A549 cells were treated with or without 2 μM arsenic for 6 h, and the protein level of A3B was analyzed by blotting assay. *C*, protein lysates prepared from (*A*) were used in an *in vitro* cytidine deaminase assay. Positions of the substrate (probe) and the deamination product are labeled. *D*, illustration of the first and second PCR primer setting for 3D-PCR of human TP53. *E*, control or A3B-depleted A549 cells after arsenic treatment were harvested for the extraction of genomic DNA, and agarose gel analysis of 3D-PCR amplicons from TP53 was then performed. The denaturation temperature range is indicated above gel. *F*, pie charts depicting the mutation degree from 3D-PCR products after cloning and sequencing. *G*, bar plots depicting the number of mutations of the indicated nucleotide from (*F*). 3D-PCR, differential DNA denaturation PCR; A3B, APOBEC3B; As, arsenic; UDG, uracil-DNA glycosylase.

generate the mutant-type constructs (A3B-M1, A3B-M2, A3B-M3, and A3B-M4). Gene-specific m6A qPCR was then performed to compare the m6A methylation level between WT-A3B and A3B-mutants in the context of A3B-deficient cells. As shown in Figure 2*F*, the A3B-M4 had significantly lower m6A signals than WT-A3B and the other three mutants, indicating that the fourth m6A RRACH motif which is located near the stop codon might be the primary m6A site in the A3B mRNA. Furthermore, A3B-M4 had higher mRNA and protein expression levels in A3B-depleted cells (Fig. 2, *G* and *I*), suggesting that m6A modification is critical for A3B expression. To verify this hypothesis, we compared the RNA half-life between WT-A3B and A3B-M4 in A3B-depleted cells. As shown in Figure 2*H*, A3B-M4 was unable to be degraded, which may lead to higher mRNA and protein levels. In addition, WT-A3B but not A3B-M4 was significantly induced by As exposure (Fig. 2*I*), suggesting that the m6A modification of A3B mRNA is indispensable for its responses to As treatment. Moreover, cytidine deaminase activity and C/G to A/T transition and transversions were much more pronounced in A3B-M4 cells compared to WT-A3B cells. More notably, the enzymatic and mutagenic activities of A3B-M4 were not further enhanced by As treatment (Fig. 2, *J* and *K*), indicating that A3B expression level and function are regulated by its m6A level under As treatment.

FTO is responsible for erasing the m6A modification of A3B

To identify which m6A modulator participated in the regulation of m6A modification of A3B, we detected the protein levels of m6A writers (METTL3, METTL1, and METTL16), erasers (FTO and ALKBH5), and readers (YTHDF2) in response to As. As shown in Figure 3*A*, the protein level of FTO, but not the other m6A modulators, was increased upon As treatment; meanwhile, the mRNA level of FTO was not changed (Fig. S2*A*), suggesting that FTO might be required for As-reduced global m6A level. In addition, RIP analysis showed that FTO was able to bind to A3B mRNA (Fig. 3*B*), suggesting that FTO is the m6A demethylase of A3B. To confirm this hypothesis, we knocked down FTO by transfection with two specific siRNAs. As shown in Fig. S2, *B* and *C* and Figure 3*C*, both the mRNA and protein levels of A3B were significantly decreased when FTO was depleted. We next investigated whether FTO removes the m6A modification from A3B mRNA through its enzymatic activity. As shown in

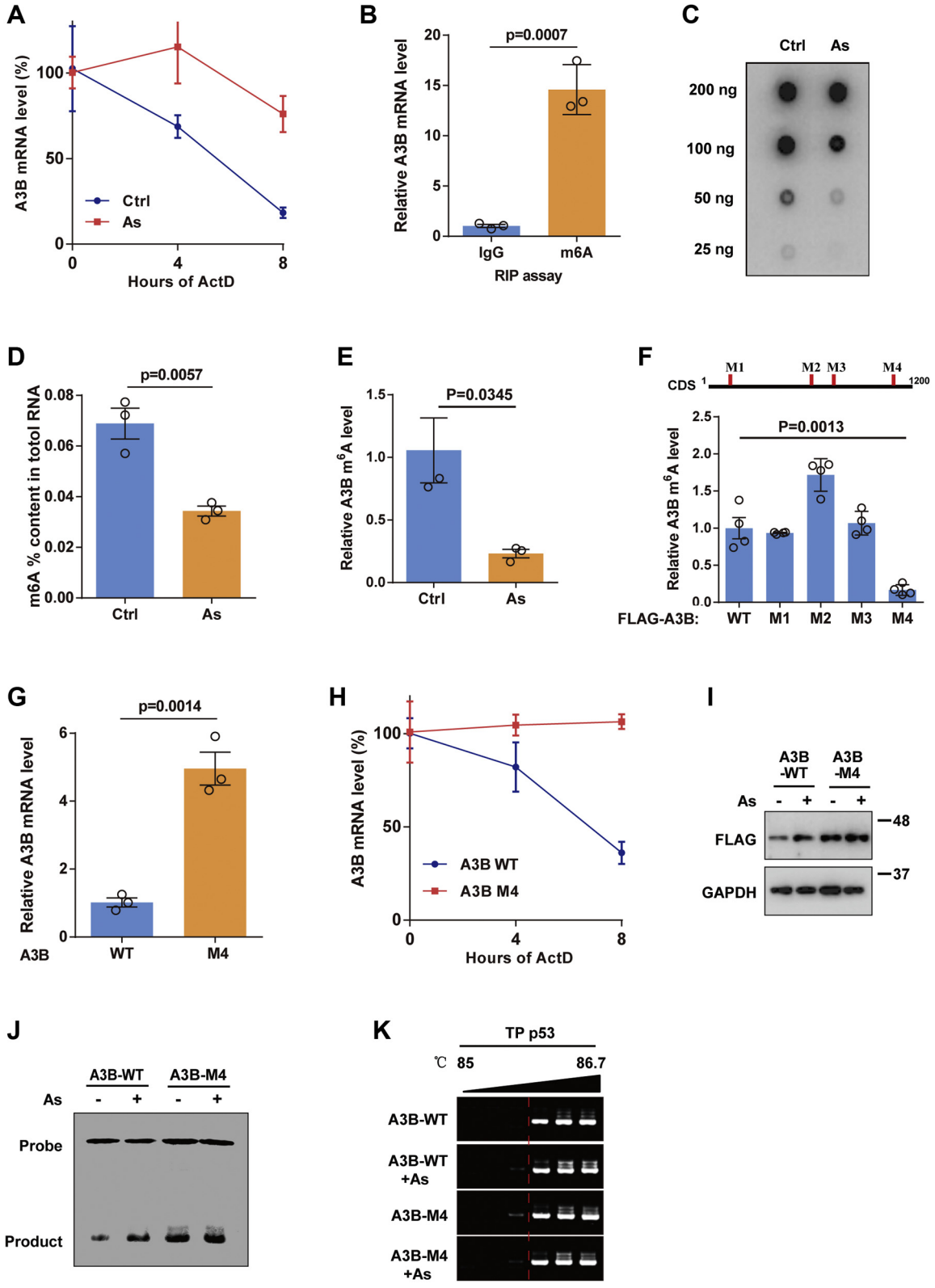

Figure 2. m6A-modified A3B mRNA is decreased after arsenic exposure and negative relevant to A3B expression. *A*, A549 cells were treated with or without 2 μM arsenic for 6 h before replaced with fresh cell culture medium, cells were then treated with 2 μM ActD for the indicated time points, and the mRNA levels of A3B were detected by qPCR analysis. *B*, RIP-qPCR showing the interaction between A3B mRNA with m6A modifications in A549 cells. *C*, m6A dot blot analysis using total RNAs derived from A549 cells that are treated with arsenic or left untreated (n = 3). *D*, total m6A methylation level was measured in A549 cells upon arsenic treatment using colorimetric m6A quantification kit (n = 3). *E*, the enrichment of m6A modification on A3B mRNA in A549 cells was detected by gene-specific m6A qPCR assay. *F*, A3B-depleted A549 cells were transfected with WT-A3B and the indicated A3B mutates for 24 h before harvested. Gene-specific m6A qPCR assay was then performed to compare the m6A modification levels on A3B mRNA. A schematic of the m6A modification sites of A3B was shown above. *G*, the mRNA levels of A3B in A3B-depleted A549 cells transfecting WT-A3B and M4-A3B were analyzed by qPCR assay. *H*, A3B-depleted A549 cells were transfected with WT-A3B and M4-A3B for 24 h before treated with 2 μM ActD for the indicated time points, and

Fig. S2, *D* and *E*, overexpressing WT FTO in FTO-knockdown cells increased the mRNA and protein levels of A3B, but overexpressing the demethylase-deficient mutant FTO (R96Q) failed to phenocopy these results. This indicated to us that the demethylase activity is required for the regulatory role of FTO in A3B expression. In addition, gene-specific m6A qPCR analysis showed that the m6A level of A3B was also markedly increased in FTO-knockdown cells (Fig. 3*D*). Moreover, co-knocking down METTL3/14 and FTO reversed FTO depletion–reduced A3B mRNA and protein expression (Fig. S2, *F* and *G*), indicating that the regulation of A3B by FTO is m6A dependent. We next assessed whether FTO regulates the mRNA fate of A3B. As shown in Figure 3*E*, the mRNA stability of A3B decreased faster when FTO was depleted. Moreover, FTO overexpression increased the protein level of WT-A3B but not A3B-M4 whose m6A motif was mutated (Fig. 3*F*), further confirming that A3B is directly regulated by FTO in an m6A-dependent manner.

To examine the biological role of FTO in m6A demethylation of A3B under As exposure, we detected the expression level of A3B in FTO-depleted cells after As treatment. As shown in Figure 3*G*, the induction of A3B was significantly impaired when FTO was depleted. Furthermore, As-induced p53 expression, γ-H2AX foci formation, and cell viability reduction were all obviously attenuated in FTO-deficient cells compared to that in control cells (Fig. S2, *H–J*). We next determined whether FTO is responsible for As-induced mutagenesis by A3B. As shown in Figure 3, *H–J*, FTO depletion significantly reduced the cytidine deaminase activity and A/T content in the 3D-PCR products under As treatment. This could be effectively reversed by A3B expression, demonstrating that A3B is an important target of FTO to promote As-induced somatic DNA mutation.

FB23-2, an FTO-specific inhibitor which directly binds to FTO and selectively inhibits FTO's m6A demethylase activity (32), was used to further verify the regulatory role of FTO in A3B expression and As-induced mutagenesis. As shown in Figure 3, *K–M*, the mRNA and protein levels of A3B were all significantly decreased in FB23-2-treated cells compared to that in dimethyl sulfoxide treated cells, while m6A modification of A3B mRNA was significantly increased. Additionally, *in vitro* cytosine deaminase and 3D-PCR analyses showed that FB23-2 pretreatment effectively inhibited As exposure–enhanced cytidine deaminase activity and A/T content in TP53 in 3D-PCR products (Fig. 3, *N* and *O*). Moreover, the sequencing results from these 3D-PCR products demonstrated that the percentages of amplicons with more mutations and C/G to T/A transitions and transversions were reduced in FB23-2 pretreated cells after As treatment (Fig. 3, *P* and *Q*). Taken together, these findings further proved that FTO is critical for As-induced mutagenesis through regulating the m6A modification of A3B.

FTO regulates the stability of A3B mRNA via *YTHDF2-dependent mechanism*

The biological importance of m6A mRNA modification is executed mostly by m6A readers that control mRNA stability, translation, splicing, or subcellular localization (33, 34). It was reported that YTHDF family members regulate the translation efficiency and mRNA stability of m6A-modified mRNA (33, 34); thus, we knocked down YTHDF1-3 with their specific siRNA and observed the consequences on A3B mRNA. As shown in Figure 4*A*, knocking down YTHDF2 but not YTHDF1 and YTHDF3 significantly increased the mRNA level of A3B. Consistently, RIP analysis showed that YTHDF2 antibody enriched more A3B mRNA than IgG (Fig. 4*B*). To test whether YTHDF2 recognizes and decays m6A-modified A3B mRNA, we compared the mRNA stability of A3B in control or YTHDF2-depleted cells. As shown in Figure 4*C*, A3B mRNA is more stable when YTHDF2 was silenced. Furthermore, knocking down YTHDF2 rescued FTO depletion–reduced A3B expression (Fig. 4, *D* and *E*), indicating that FTO regulates A3B expression in an m6A-YTHDF2-dependent manner.

To explore the crucial function of FTO/YTHDF2 m6A axis in As-induced DNA damage and mutation, we knocked down YTHDF2 in FTO and UNG depletion cells before As treatment. As shown in Fig. S3, *A–D*, knocking down YTHDF2 remarkably reversed FTO depletion–reduced γ-H2AX foci formation and FTO depletion–increased cell viability under As treatment. In addition, knocking down YTHDF2 increased the cytosine deaminase activity of lysates prepared from FTO-deficient cells under As treatment (Fig. 4*F*), indicating that YTHDF2 plays a suppressor role in the enzymatic activity of A3B by decaying its m6A-modifed mRNA. Furthermore, we used 3D-PCR assay to analyze whether YTHDF2 affects the DNA editing ability of A3B in FTO-depleted cells. As shown in Figure 4, *G–I*, FTO depletion–reduced DNA hypermutation under As exposure could be rescued by co-knockdown YTFDF2. Moreover, the percentage of A/T-rich DNA after As treatment was also increased in the combination of FTO- and YTHDF2-depleted cells than that in FTO-deficient cells. These data indicate that A3B-mediated DNA damage and hypermutation under As treatment is controlled by the FTO/YTHDF2 m6A axis.

As exposure induces the activation of FTO/APOBEC3 pathway in vivo

Because there is a similar high confidence m6A motif (mGGACA *versus* hGGACU) near the stop codon of mouse *Apobec3* CDS region, we inferred that FTO might also regulate the expression of *Apobec3*. Therefore, we examined the relationship between FTO and APOBEC3 after As treatment in mouse Lewis lung carcinoma cells (LLC1). As shown in Figure 5, *A* and *B*, As treatment induced an increase of

qPCR analysis was then performed to detect the mRNA stability of A3B. *I–K*, A3B-depleted A549 cells were transfected with WT-A3B and M4-A3B for 24 h before in response to arsenic for 6 h. The protein level of A3B was analyzed by Western blotting assay (*I*); protein lysates were used for *in vitro* cytidine deaminase assay (*J*); genomic DNA was extracted for TP53 3D-PCR amplicons and analyzed by agarose gel (*K*). 3D-PCR, differential DNA denaturation PCR; A3B, APOBEC3B; ActD, actinomycin D; As, arsenic; m6A, N6-methyladenosine; RIP, RNA immunoprecipitation.

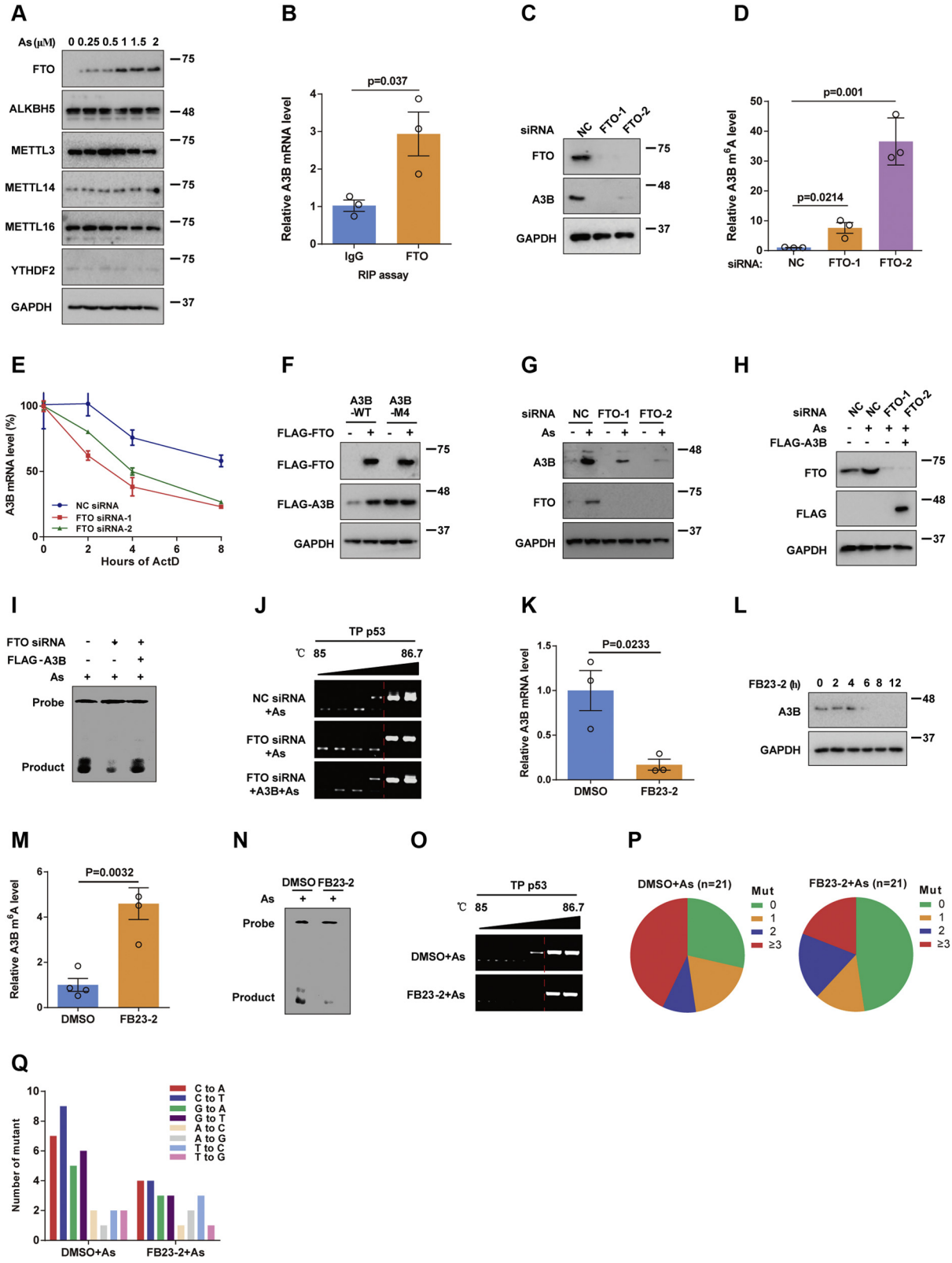

Figure 3. FTO regulates A3B expression in an m6A-dependent manner. *A*, A549 cells were untreated or treated with 2 μM arsenic for the indicated time points, and cell lysates were then immunoblotted with indicated antibodies. *B*, RIP assay was performed using IgG or FTO antibody. The enrichment of A3B mRNA was measured by qRT-PCR assay (n = 3). *C*, Western blotting analysis of FTO and A3B expression levels in A549 cells transfected with NC siRNA, FTO siRNA-1, or FTO siRNA-2. *D*, gene-specific m6A qPCR analysis of the m6A enrichment on A3B mRNA in A549 cells with NC siRNA or FTO siRNA (n = 3). *E*, qRT-PCR analysis of the mRNA stability of A3B in A549 cells with or without FTO knockdown after ActD treatment (n = 3). *F*, A3B-depleted A549 cells were pretransfected with vector or FLAG-FTO for 24 h and then transfected with WT-A3B and M4-A3B for 24 h to detect the expression level of exogenous FTO and A3B by Western blotting assay. *G*, control and FTO-depleted A549 cells were treated with 2 μM arsenic for 6 h, and the expression of FTO and A3B was then analyzed by immunoblotting assay. *H–J*, NC or FTO siRNA-transfected A549 cells were transfected with FLAG-A3B for 24 h before in response to

Apobec3 mRNA and protein levels, which was effectively inhibited by FB23-2. Next, *in vivo* experiments were performed to analyze the activation of the FTO/APOBEC3 pathway in the lung tissues of C57BL/6 mice after inhalation of aerosolized PBS or As. As shown in Figure 5, *C–E*, As mass and γ-H2AX foci formation in the lung tissues of As-exposed mice were significantly increased compared to that in PBS-treated mice, whereas the degree of DNA damage was impaired in FB23-2 pretreated group. Meanwhile, the induction of APOBEC3 was also inhibited with FB23-2 pretreatment in lung tissues of mice after As treatment (Fig. 5, *F* and *G*), indicating that As induces the activation of FTO/A3B pathway to promote DNA damage *in vivo*.

FTO is upregulated in human lung cancer and correlated with A3B expression

It was reported that both FTO and A3B play oncogenic roles in the progression of lung cancer (3, 35); thus, we investigate the correlation between FTO and A3B in human lung cancers. Through the analysis of the lung tissue microarrays including 52 lung tumor samples and 52 normal tissues adjacent to the tumor, we found that both FTO and A3B are overexpressed in lung tumors compared to normal adjacent tissues (Fig. 6, *A* and *B*). In addition, 61.5% (32/52) of FTO-high tumor samples had high level of A3B, and there has a significant positive correlation between FTO and A3B (p = 0.001, Pearson R = 0.475) (Fig. 6*C*). Representative images of FTO and A3B staining in lung tumor cases with high or low FTO and A3B expression are shown in Figure 6*D*. In addition, clinical data suggest that the upregulation of FTO and A3B expression was significantly related to shorter overall survival in lung cancer (Fig. 6, *E* and *F*). These data indicate that the expression of FTO is closely correlated with A3B and poor prognosis in lung cancer, further confirming the significance of FTO/A3B axis in lung tumor progression.

Discussion

Cytidine deaminase APOBEC family members, especially A3B, are upregulated and play a critical role in the mutation and evolution process of cancers which carry a heavy mutation load (3, 36). However, it remains challenging to reveal the precise mechanism by which A3B is induced; thus, there is a shortage of reliable strategies for targeting cancers overexpressing A3B. Here, our data show that FTO is upregulated and promotes A3B expression in an m6A-YTHDF2-dependent manner under As treatment, resulting in increased somatic mutations and DNA damage, which reveal the regulatory mechanism of A3B expression under As stress and suggest that FTO inhibitor might be a potential treatment choice for tumors overexpressing A3B.

A3B expression is reported to be induced by replication stress and chemotherapy drugs, thereafter leading to potent DNA damage and base substitutions in the genome (12, 13, 37). In addition, A3B overexpression causes uracil lesion accumulation in UNG-depleted cells, which results in cell death in p53-dependent manner (8). As is a well-known DNA damage inducer and exogenous carcinogen which causes replication-dependent DNA breakage and oxidative DNA damage (28, 38). However, the precise mechanism of As-induced mutagenesis has not been clearly described. Our results showed that A3B expression is critical for As-triggered mutagenesis, which provides a novel insight for the understanding of As-induced genome instability. As provokes numerous toxic effects in mammalian cells by activating a variety of signaling pathways (39); our results suggested that A3B induction might be partly responsible for As-induced DNA damage and cell death effect. However, the detailed mechanism linking A3B-mediated mutagenesis to DNA double-strand breaks and reduced cell viability under low-dose As exposure is still elusive and needs further study.

It has been reported that m6A modification in RNA is an early step of the DNA damage response (40–43). For example, METTL3/14 and FTO transiently and dynamically regulate m6A modification at DNA damage sites and then recruit Pol κ to facilitate DNA repair following UV exposure (40). During homologous recombination repair, m6A methylation on R-loops is catalyzed by METTL3 which is required for the removal of R-loops in YTHDC1-dependent manner (41). Reactive oxygen species enhances the global mRNA m6A levels by regulating ALKBH5 SUMOylation to quickly induce DNA damage repair gene expression (42). FTO increases mRNA stability of Hspa1a and DNA repair genes to promote resistance to UV and H2O2-induced DNA damage and cell apoptosis (43). Our data demonstrate that m6A modification also plays an important role in As-induced DNA mutation by regulating the mRNA stability of A3B. The m6A motif is located near the stop codon of the CDS region in A3B mRNA which could be catalyzed by METTL3/14, and the m6A modified-A3B is then recognized and decayed by YTHDF2 to avoid uncontrolled DNA mutation under physiological condition. However, after As exposure, upregulated FTO removes the m6A modification from A3B mRNA to enhance its mRNA stability, leading to increased A3B expression and DNA mutation rate. Our studies thus illustrate a novel role of m6A in the regulation of DNA mutation triggered by exogenous DNA damaging stresses. In addition, we also confirmed the activation of the FTO/APOBEC3 pathway in mouse lung adenocarcinoma cells and mice lung tissues after As exposure, implying that the effect of As on the FTO/A3B

arsenic. Cell lysates were then used for immunoblotting assay with indicated antibodies (*H*) or *in vitro* cytidine deaminase assay (*I*); the genomic DNA was used for the analysis of TP53 by 3D-PCR amplicons (*J*). *K*, A549 cells were treated with DMSO or 10 μM FB23-2 for 12 h and then the mRNA level of A3B was measured by qPCR assay. *L*, A549 cells were treated with 10 μM FB23-2 for the indicated time points, and the expression level of A3B was analyzed by immunoblotting assay. *M*, gene-specific m6A qPCR analysis of the m6A modification level of A3B in A549 cells treated with DMSO or FB23-2 (n = 3). *N*, cytidine deamination activities of the cell lysates derived from DMSO-pretreated or FB23-2-pretreated A549 cells when under arsenic exposure. *O*, A549 cells were treated with DMSO or FB23-2 for 1 h before arsenic treatment, and TP53 was then amplified by 3D-PCR and analyzed by agarose gel. *P* and *Q*, pie charts depicting the mutation degree (*P*) or bar plots depicting the number of mutations of the indicated nucleotide (*Q*) from 3D-PCR products. 3D-PCR, differential DNA denaturation PCR; A3B, APOBEC3B; ActD, actinomycin D; RIP, RNA immunoprecipitation.

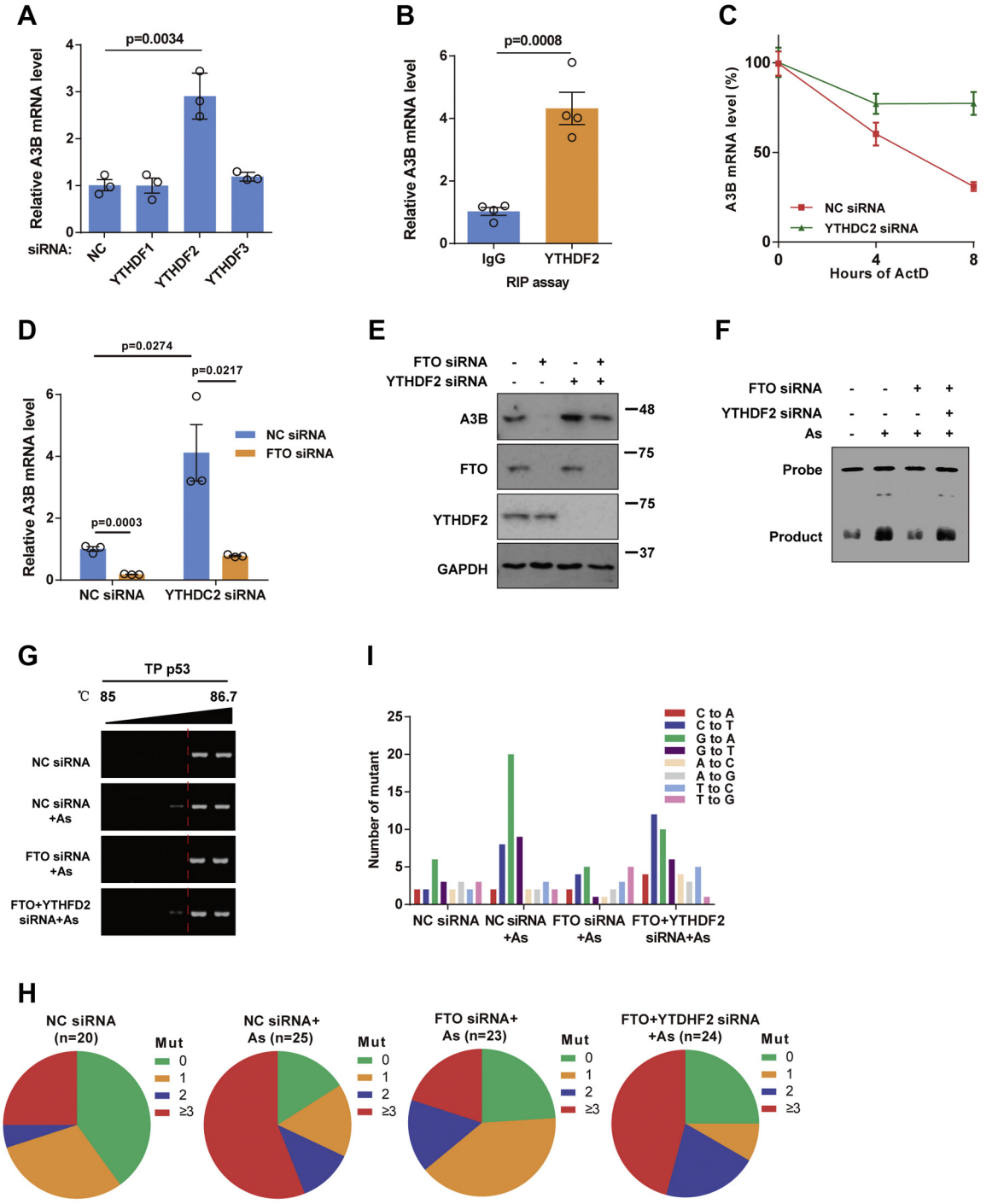

Figure 4. FTO regulates A3B expression by inhibiting m6A/YTHDF2-mediated mRNA decay. *A*, qPCR analysis of the mRNA levels of A3B in A549 cells transfecting with NC or YTHDF1-3 siRNAs. *B*, RIP-qPCR was used to detect the enrichment of YTHDF on A3B mRNA (n = 3). *C*, qPCR analysis of the stability of A3B mRNA in NC-transfected or YTHDF2 siRNA–transfected cells when treated with ActD for the indicated time points. *D* and *E*, A549 cells were transfected with NC siRNA, FTO siRNA, or YTHDF2 siRNA or cotransfected with FTO and YTHDF2 siRNA for 72 h, and the mRNA and protein levels of A3B were then analyzed by qPCR assay (*D*) and immunoblotting assay (*E*), respectively. *F–I*, A549 cells were transfected with NC siRNA, FTO siRNA, or in combination of FTO and YTHDF2 siRNAs for 60 h before in response to arsenic. Cell lysates were used for *in vitro* cytidine deaminase assay (*F*); genomic DNA was used for TP53 3D-PCR amplicons and analyzed by agarose gel (*G*); pie charts depicting the mutation degree (*H*) or bar plots depicting the number of mutations in TP53 detected by sequencing 3D-PCR products (*I*). 3D-PCR, differential DNA denaturation PCR; A3B, APOBEC3B; ActD, actinomycin D; As, arsenic; RIP, RNA immunoprecipitation.

axis activation in the lung is universal and physiological. Recently, another article reported that FTO is induced through the inhibition of p62-mediated selective autophagy under low-level As exposure and required for As-induced skin tumorigenesis by regulating the expression of NEDD4L (44), consistent with our conclusion that FTO is a critical regulator for As tumorigenesis but through different point of view and molecular mechanism.

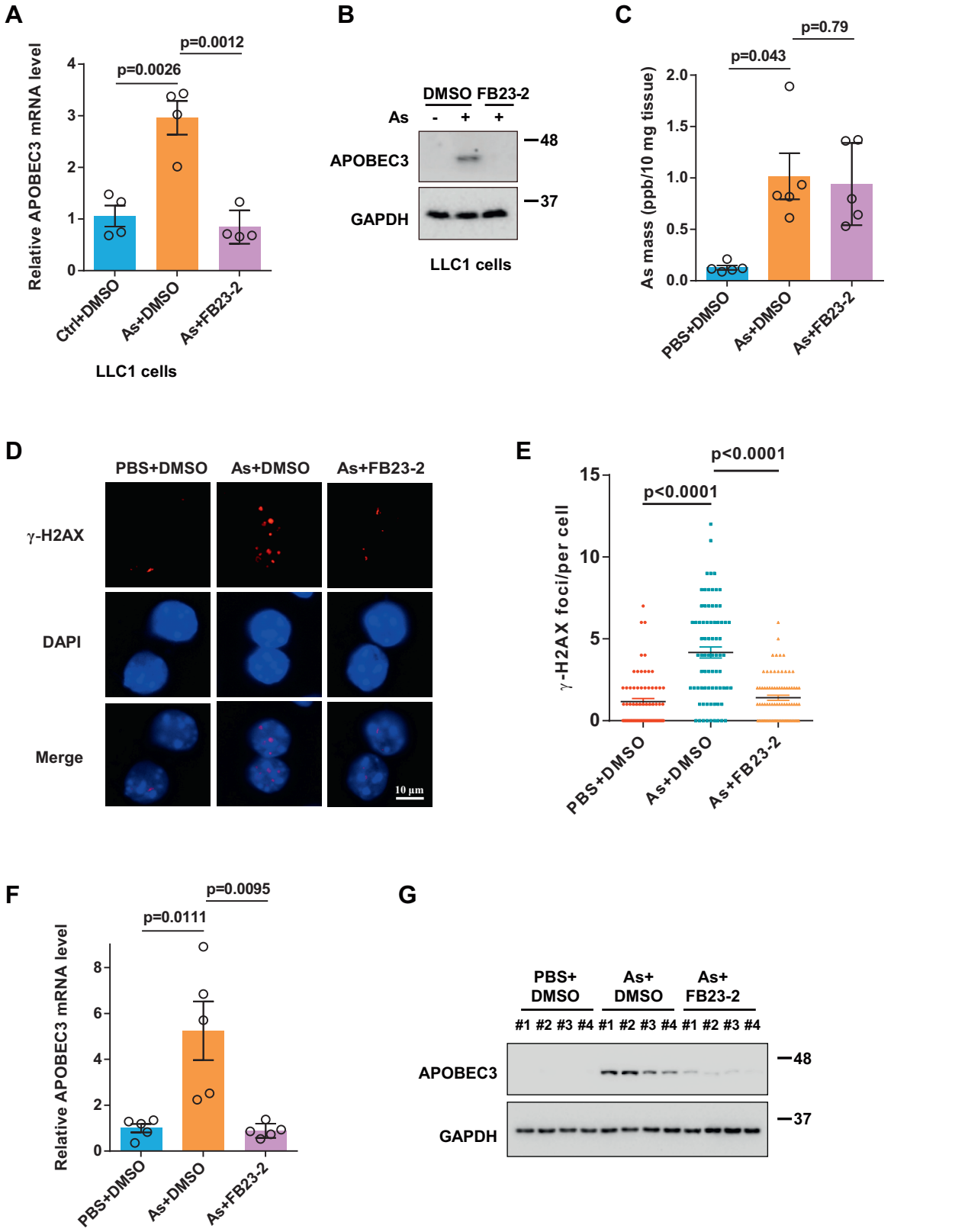

Figure 5. The FTO/APOBEC3 axis is increased upon arsenic treatment in LLC1 cells and *in vivo*. *A* and *B*, LLC1 cells were pretreated with FB23-2 and then added with 2 μM arsenic for 6 h, and the mRNA and protein levels of APOBEC3 were detected by qPCR and Western blotting analysis. *C–E*, C57BL/6 mice with or without 5 mg/kg FB23-2 pretreatment were inhaled aerosolized PBS or 0.5 mg/kg arsenic for 48 h. The content of arsenic in the lung tissue were determined by ICP-MS assay (n = 4) (*C*). The γ-H2AX signals from the lung tissues were detected by immunofluorescence assay, and representative images and quantification are shown in (*D*) and (*E*), respectively (n = 4). *F* and *G*, the mRNA level and protein levels of A3B in the lung tissues of mice were detected by qRT-PCR and immunoblotting assay (n = 4), respectively. Error bars represent ±SEM from this experiment. As, arsenic; ICP-MS, inductively coupled plasma MS.

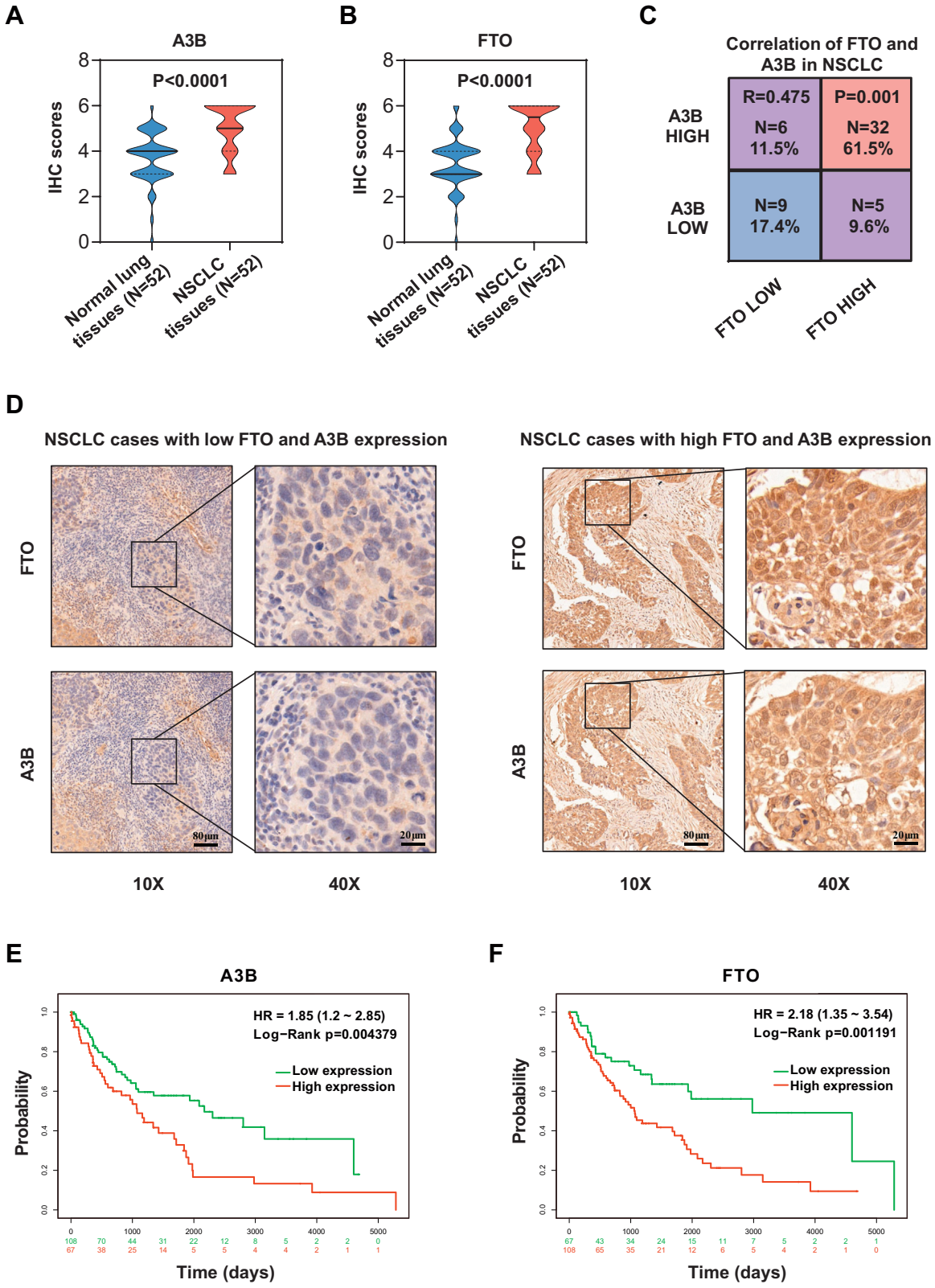

Figure 6. FTO expression is correlated with A3B levels in human lung cancer. *A* and *B*, the IHC score of A3B and FTO was significantly higher in lung cancer tissues compared with that in adjacent normal tissues. *C*, FTO expression correlates with A3B levels in lung cancer tissue microarray. Statistical analyses were performed with the χ^2 test. *D*, representative images of the immunohistochemical staining of high FTO and A3B expression or low FTO and A3B expression on tissue microarray of lung cancer specimens (n = 52). *E* and *F*, survival analyses of lung cancer patients with higher A3B or FTO expression by the Kaplan–Meier Plotter. A3B, APOBEC3B; NSCLC, non–small cell lung cancer.

It has been reported that FTO inhibitor FB23-2 specifically results in a substantial increase of cellular m6A in acute myelocytic leukemia cells (32). In addition, other types of RNAs such as microRNAs, long noncoding RNAs, and circular RNAs are also dynamically regulated by m6A modification (45–48). Thus, it is possible that FTO regulates biological process through simultaneity control of many downstream target genes expression in directly and indirectly manners. Herein, we performed RIP assay, m6A site mutation assay, and rescue assay to substantiate that FTO directly binds at the stop codon region of A3B, thereafter promoting As-induced A3B expression and DNA mutation. However, we cannot exclude the possibility that FTO also increases the expression levels of A3B upstream regulators such as NF-κB and E2F family members or FTO regulates other DNA mutation drivers such as adenosine deaminase to a lesser extent to promote As-induced mutagenesis, which needs further investigation in the future.

It was reported that spontaneous mutation rate in humans is estimated 10^{-4} to 10^{-6} per gene per generation, and the p53 gene mutation is found in about 50 to 60% of human cancers (49). DNA damage induced by replication, mutagenesis, or environmental stress can be recognized and corrected by the DNA damage repair systems such as base excision repair (50). However, several toxic environmental factors can cause more DNA mutations that overwhelm the capacity of the DNA repair system and leave many mutations unfixed, which affects genome integrity and stability (51). Because of lack of DNA repair system in PCR reaction, the Taq DNA polymerase which is used for PCR amplification might lead to more mutations (estimated about 4×10^{-7}–2×10^{-5} error frequencies) (52). In addition, the PCR reaction efficacy and accuracy are also affected by the sequence and structure of DNA template as well as the reaction temperature. Therefore, the DNA mutation rate in 3D-PCR assay is higher than spontaneous mutation even in untreated cells. Although the DNA mutation rate from 3D-PCR can partially represent the mutagenesis activity triggered by A3B, under the depletion of UNG, the future work should be explored to detect the DNA mutation rate induced by low-dose As using whole exome sequencing.

In summary, we have elucidated how cancer cells coordinate mutation drivers and m6A modification to promote As-induced carcinogenesis. Our data highlight the functional importance of m6A modification machinery in modulating As-induced DNA mutation by regulating A3B expression in an m6A-dependent mechanism and provide a promising therapeutic strategy for lowering DNA mutation rates in cancer cells.

Experimental procedures

Cell culture

Human lung adenocarcinoma cells A549 and mouse Lewis lung carcinoma cells LLC1 were purchased form the Cell Resource Center of the Institute of Basic Medical Sciences (CAMS). Cells were characterized by DNA fingerprinting and isozyme detection. Cells were maintained in Dulbecco's modified Eagle's medium with 10% fetal bovine serum and kept in a humidified 37 °C incubator with 5% CO_2.

Plasmids, reagents, and antibodies

FLAG-tagged full length and the mutants of FLAG-A3B were amplified and integrated into pLVX-3Flag vector. FLAG-FTO was purchased from Sino Biological Inc. FLAG-FTO R96Q was generated by site-directed mutagenesis (NEB). As, FB23-2, Actinomycin D, and DAPI were purchased from Sigma Aldrich. Anti-ALKBH5, METTL3, METTL14, METTL16, YTHDF2, p53, and GAPDH were purchased from ProteinTech Group; anti-γH2AX (phospho-ser139) was obtained from Millipore; anti-FLAG antibody was purchased from Sigma; anti-A3B and FTO were purchased from CST.

RNA interference

The siRNAs targeting FTO, METTL3, METTL14, YTHDF1-3, and A3B shRNA lentivirus were purchased from GenePharma. siRNAs were transfected into cells using Lipofectamine 2000 transfection reagent (Invitrogen) according to the manufacturer's instruction.

Western blotting assay

Cells were lysed with NETN buffer (20 mM Tris–HCl, pH 8.0, 100 mM NaCl, 1 mM EDTA, 0.5% Nonidet P-40 with protease inhibitor cocktails) for 30 min before centrifugation. Supernatant was then mixed with 2× Laemmli buffer and subjected to SDS-PAGE separation, thereafter detected with indicated antibodies.

Colony formation assay

One thousand A549 cells transfecting the indicated siRNAs or shRNAs were seeded into 6-well plates for 48 h before treated with As for about 2 weeks. Colonies were then stained with 5% Giemsa and counted.

Immunofluorescence

A549 cells transfecting the indicated siRNAs or shRNAs for 48 h were plated on coverslips for 24 h before in response to As. Cells were then fixed using 4% paraformaldehyde for 20 min at room temperature and then washed three times before permeabilized with 0.1% Triton-X solution for 10 min. Cells were blocked with 5% goat serum for 30 min before incubated with anti-γH2AX (phospho-ser139) at 4 °C overnight. Subsequently, cells were washed again and incubated with Alexa Fluor 488-conjugated second primary antibodies for 1 h at room temperature. Nuclear DNA was stained with DAPI and then the formation of γ-H2AX foci was detected by the confocal laser scanning.

Cytidine deaminase activity assay

Cells were lysed with NETN buffer for 30 min, and 10 μg lysate was incubated with 2 μg RNase A in 50 μl volume at 37 °C for 15 min, and 2 μg RNase A-treated lysate was mixed with 1 pmol ssDNA substrate 5′ Cy5-ATT ATT ATT ATT

ATT ATT ATT TCA TTT ATT TAT TTA TTT A-3′ and 0.75 unit uracil–DNA glycosylase (NEB) in 40 μl reaction volume at 37 °C for 30 min. Thereafter added with 10 μl 1N NaOH and incubated for additional 15 min at 37 °C, which was then neutralized by 10 μl 1N HCl. Samples are mixed in 2× TBE urea sample buffer and heated at 90 °C for 5 min before separated on 15% urea-PAGE gel in TBE buffer. Gel is imaged on Odyssey FC scanner.

3D-PCR and sequencing

UNG-depleted A549 cells were treated with 2 μM As for 1 week before harvested for 3D-PCR assay. Genomic DNA was extracted by DNAzol reagent (ThermoFisher Scientific) and then 3D-PCR was performed to amplify p53 genes as described (9). For Sanger sequencing, amplicons derived at the lowest temperature were cloned into pGEM-T Easy plasmids (TaKaRa) and then sequenced. The Sanger sequencing raw data on 3D-PCR are shown in the supplementary materials.

Quantitative real-time PCR (qRT-PCR)

Total RNA was extracted by Trizol (Invitrogen), and cDNA was synthesized using First Strand cDNA Synthesis Kit (Toyobo) according to the manufacturer's instruction. qPCR was then performed on an iQ5 PCR instrument (Bio-Rad), as described (53).

RIP assay

RIP assay was performed as described (53). Briefly, A549 cells were lysed with RIP lysis buffer for 30 min; 2 μg indicated antibodies and normal rabbit IgG were incubated with Magnetic Beads Protein A/G for 1 h before mixed with cell lysate overnight at 4 °C. Pull-down lysate was digested with proteinase K and then RNAs were extracted with phenol–chloroform–isoamyl alcohol (25:24:1), and the binding RNAs were analyzed by qRT-PCR assay.

m6A dot blot assay

Total RNA was used to conduct m6A dot blot assays. In brief, 2 μl samples were loaded onto a nitrocellulose membrane (Millipore) and then crosslinked by UV. The membrane was blocked before incubated with anti-m6A antibody overnight at 4 °C, followed by horseradish peroxidase conjugated secondary antibody for 1 h at room temperature, and then developed with ECL reagent (ThermoFisher Scientific).

Gene-specific m6A qPCR

Polyadenylated RNA was extracted using Dynabeads mRNA Purification Kit (Life Technology). Thereafter 50 ng mRNA was saved as input, and about 1 μg mRNA was incubated with m6A antibody (Synaptic Systems) and then rotated in 500 μl volume IP buffer (150 mM NaCl, 0.1% NP-40, 10 mM Tris, pH 7.4, 100 U RNase inhibitor) at 4 °C for 2 h, Dynabeads Protein A (MCE) was then added and rotated for another 2 h at 4 °C. After washed four times using IP buffer, the m6A-IPed mRNA was eluted twice by 50 μl m6A-elute buffer (IP buffer, 6.7 mM m6A, 30 U RNase inhibitor) and then purified by ethanol precipitation. qPCR was performed to determine the levels of A3B mRNA in m6A antibody-IPed samples and input samples.

Mouse treatment

All animal studies were approved by the Ethical Review Board of the Research Center for Eco-Environmental Sciences, Chinese Academy of Sciences. Six 8-week-old female C57BL/6 mice, about 18 to 20 g per mice, were randomized into two groups: dimethyl sulfoxide and FB23-2 (5 mg/kg) and then mice were inhaled aerosolized 0.5 mg/kg As or PBS using an air-compressing nebulizer. After 48 h, mice were sacrificed and then the As mass, γ-H2AX foci formation, and A3B expression levels were determined.

Inductively coupled plasma MS analysis

The lung tissues of mice were digested with mixed acid using a microwave on a MARS machine (CEM Corp) for 24 h. The As mass in the tissues was determined by inductively coupled plasma MS using a quadrupole inductively coupled plasma mass spectrometer (Agilent), as described (53).

Tissue microarray

The tissue microarrays of lung cancer specimen were purchased from Shanghai Outdo Biotech (OD-CT-RsLug04-004). In brief, tissue microarrays were placed in xylene (5 min, twice), anhydrous ethanol (3 min, twice), 95% ethanol (3 min, once), 90% ethanol (3 min, once), and distilled water (3 min, twice). Then, the microarrays are placed in 1% hydrogen peroxide and incubated at room temperature in darkness for 40 min before placed in a repair box filled with citric acid at pH 6.0. The microarrays were then washed twice before sealed with 3% bovine serum albumin for 1 h at room temperature. Microarrays were then incubated with antibodies overnight at 4 °C. Washed twice and then incubated with horseradish peroxidase-conjugated secondary antibody for 1 h at room temperature. Diaminobenzidine solution was then applied to the sections for 15 to 20 s to develop the peroxidase reaction product. Immunohistochemistry staining of the biomarkers was evaluated by the German semi-quantitative scoring system which is according to the staining intensity (no staining, weak staining, moderate staining, and strong staining were allotted scores of 0, 1, 2, and 3, respectively) and the percentage of positive cells (≤5% positive cells, 6–25% positive cells, 26–50% positive cells, and >50% positive cells were allotted scores of 0, 1, 2, and 3, respectively). Protein expression scores for the staining intensity and the percentage of positive cells were added. Protein expression levels were dichotomized as low expression (scored 0–4) and high expression (scored 5–6). Remarks: Pearson R = 0.475; Fisher's exact test (p = 0.001).

Statistics

Data in bar and line graphs are presented as mean ± SEM of three independent experiments. Statistical analyses were performed with the Student's t test.

Data availability

Research data are available upon request. No data were deposited to databases.

Supporting information—This article contains supporting information.

Acknowledgments—This research was supported by the National Natural Science Foundation of China (Grant No. 22076212), the Strategic Priority Research Program of the Chinese Academy of Sciences (XDPB2004), the China National Key R&D Program (2021YFA0719300), the Science Fund for Creative Research Groups of the National Natural Science Foundation of China (22021003), and the Youth Innovation Promotion Association of CAS (2021040).

Author contributions—M. G., Z. Q., Jinzhou Huang, Z. L., and S. L. conceptualization; M. G., Z. Q., Jinzhou Huang, Z. L., and S. L. methodology; M. G. and Z. Q. investigation; M. G., Z. Q., W. F., H. H., Z. X., Z. D., M. X., and Jinxiang Han validation; M. G., Z. Q., W. F., H. H., Z. X., Z. D., M. X., Jinxiang Han, J. A. K., Jinzhou Huang, Z. L., and S. L. formal analysis; Jinzhou Huang, Z. L., and S. L. supervision; W. F., H. H., Z. X., Z. D., M. X., and Jinzhou Huang software; Jinzhou Huang, Z. L., and S. L. project administration; M. G. and Z. Q. writing–original draft; J. A. K., Jinzhou Huang, Z. L., and S. L. writing-reviewing and editing; Jinzhou Huang, Z. L., and S. L. funding acquisition.

Conflict of interest—The authors declare that they have no conflicts of interest with the contents of this article.

Abbreviations—The abbreviations used are: 3D-PCR, differential DNA denaturation PCR; A3B, APOBEC3B; ActD, actinomycin D; m6A, N6-methyladenosine; NSCLC, non–small cell lung cancer; RIP, RNA immunoprecipitation.

References

1. Rotow, J., and Bivona, T. G. (2017) Understanding and targeting resistance mechanisms in NSCLC. *Nat. Rev. Cancer* **17**, 637–658
2. Herbst, R. S., Morgensztern, D., and Boshoff, C. (2018) The biology and management of non-small cell lung cancer. *Nature* **553**, 446–454
3. Wang, S., Jia, M., He, Z., and Liu, X. S. (2018) APOBEC3B and APOBEC mutational signature as potential predictive markers for immunotherapy response in non-small cell lung cancer. *Oncogene* **37**, 3924–3936
4. Green, A. M., and Weitzman, M. D. (2019) The spectrum of APOBEC3 activity: From anti-viral agents to anti-cancer opportunities. *DNA Repair (Amst.)* **83**, 102700
5. Salter, J. D., Bennett, R. P., and Smith, H. C. (2016) The APOBEC protein family: United by structure, divergent in function. *Trends Biochem. Sci.* **41**, 578–594
6. Roberts, S. A., Sterling, J., Thompson, C., Harris, S., Mav, D., Shah, R., Klimczak, L. J., Kryukov, G. V., Malc, E., Mieczkowski, P. A., Resnick, M. A., and Gordenin, D. A. (2012) Clustered mutations in yeast and in human cancers can arise from damaged long single-strand DNA regions. *Mol. Cell* **46**, 424–435
7. Nik-Zainal, S., Alexandrov, L. B., Wedge, D. C., Van Loo, P., Greenman, C. D., Raine, K., Jones, D., Hinton, J., Marshall, J., Stebbings, L. A., Menzies, A., Martin, S., Leung, K., Chen, L., Leroy, C., *et al.* (2012) Mutational processes molding the genomes of 21 breast cancers. *Cell* **149**, 979–993
8. Serebrenik, A. A., Starrett, G. J., Leenen, S., Jarvis, M. C., Shaban, N. M., Salamango, D. J., Nilsen, H., Brown, W. L., and Harris, R. S. (2019) The deaminase APOBEC3B triggers the death of cells lacking uracil DNA glycosylase. *Proc. Natl. Acad. Sci. U. S. A.* **116**, 22158–22163
9. Burns, M. B., Lackey, L., Carpenter, M. A., Rathore, A., Land, A. M., Leonard, B., Refsland, E. W., Kotandeniya, D., Tretyakova, N., Nikas, J. B., Yee, D., Temiz, N. A., Donohue, D. E., McDougle, R. M., Brown, W. L., *et al.* (2013) APOBEC3B is an enzymatic source of mutation in breast cancer. *Nature* **494**, 366–370
10. Buisson, R., Lawrence, M. S., Benes, C. H., and Zou, L. (2017) APOBEC3A and APOBEC3B activities render cancer cells susceptible to ATR inhibition. *Cancer Res.* **77**, 4567–4578
11. Hoopes, J. I., Cortez, L. M., Mertz, T. M., Malc, E. P., Mieczkowski, P. A., and Roberts, S. A. (2016) APOBEC3A and APOBEC3B preferentially deaminate the lagging strand template during DNA replication. *Cell Rep.* **14**, 1273–1282
12. Cescon, D. W., and Haibe-Kains, B. (2016) DNA replication stress: A source of APOBEC3B expression in breast cancer. *Genome Biol.* **17**, 202
13. Periyasamy, M., Singh, A. K., Gemma, C., Farzan, R., Allsopp, R. C., Shaw, J. A., Charmsaz, S., Young, L. S., Cunnea, P., Coombes, R. C., Győrffy, B., Buluwela, L., and Ali, S. (2021) Induction of APOBEC3B expression by chemotherapy drugs is mediated by DNA-PK-directed activation of NF-κB. *Oncogene* **40**, 1077–1090
14. Walker, B. A., Wardell, C. P., Murison, A., Boyle, E. M., Begum, D. B., Dahir, N. M., Proszek, P. Z., Melchor, L., Pawlyn, C., Kaiser, M. F., Johnson, D. C., Qiang, Y. W., Jones, J. R., Cairns, D. A., Gregory, W. M., *et al.* (2015) APOBEC family mutational signatures are associated with poor prognosis translocations in multiple myeloma. *Nat. Commun.* **6**, 6997
15. Chou, W. C., Chen, W. T., Hsiung, C. N., Hu, L. Y., Yu, J. C., Hsu, H. M., and Shen, C. Y. (2017) B-Myb induces APOBEC3B expression leading to somatic mutation in multiple cancers. *Sci. Rep.* **7**, 44089
16. Mori, S., Takeuchi, T., Ishii, Y., and Kukimoto, I. (2015) Identification of APOBEC3B promoter elements responsible for activation by human papillomavirus type 16 E6. *Biochem. Biophys. Res. Commun.* **460**, 555–560
17. Lucifora, J., Xia, Y., Reisinger, F., Zhang, K., Stadler, D., Cheng, X., Sprinzl, M. F., Koppensteiner, H., Makowska, Z., Volz, T., Remouchamps, C., Chou, W. M., Thasler, W. E., Hüser, N., Durantel, D., *et al.* (2014) Specific and nonhepatotoxic degradation of nuclear hepatitis B virus cccDNA. *Science* **343**, 1221–1228
18. Fu, Y., Dominissini, D., Rechavi, G., and He, C. (2014) Gene expression regulation mediated through reversible m^{6}A RNA methylation. *Nat. Rev. Genet.* **15**, 293–306
19. He, L., Li, H., Wu, A., Peng, Y., Shu, G., and Yin, G. (2019) Functions of N6-methyladenosine and its role in cancer. *Mol. Cancer* **18**, 176
20. Jia, G., Fu, Y., Zhao, X., Dai, Q., Zheng, G., Yang, Y., Yi, C., Lindahl, T., Pan, T., Yang, Y. G., and He, C. (2011) N6-methyladenosine in nuclear RNA is a major substrate of the obesity-associated FTO. *Nat. Chem. Biol.* **7**, 885–887
21. Wang, Y., Su, X., Zhao, M., Xu, M., Chen, Y., Li, Z., and Zhuang, W. (2021) Importance of N(6)-methyladenosine RNA modification in lung cancer (review). *Mol. Clin. Oncol.* **14**, 128
22. Chen, X. Y., Zhang, J., and Zhu, J. S. (2019) The role of m(6)A RNA methylation in human cancer. *Mol. Cancer* **18**, 103
23. Du, Y. D., Guo, W. Y., Han, C. H., Wang, Y., Chen, X. S., Li, D. W., Liu, J. L., Zhang, M., Zhu, N., and Wang, X. (2021) N6-methyladenosine demethylase FTO impairs hepatic ischemia-reperfusion injury via inhibiting Drp1-mediated mitochondrial fragmentation. *Cell Death Dis.* **12**, 442
24. Mathiyalagan, P., Adamiak, M., Mayourian, J., Sassi, Y., Liang, Y., Agarwal, N., Jha, D., Zhang, S., Kohlbrenner, E., Chepurko, E., Chen, J., Trivieri, M. G., Singh, R., Bouchareb, R., Fish, K., *et al.* (2019) FTO-dependent N(6)-methyladenosine regulates cardiac function during remodeling and repair. *Circulation* **139**, 518–532
25. Cheung, M. K., Gulati, P., O'Rahilly, S., and Yeo, G. S. (2013) FTO expression is regulated by availability of essential amino acids. *Int. J. Obes. (Lond.)* **37**, 744–747
26. Faulds, K. J., Egelston, J. N., Sedivy, L. J., Mitchell, M. K., Garimella, S., Kozlowski, H., D'Alessandro, A., Hansen, K. C., Balsbaugh, J. L., and

Phiel, C. J. (2018) Glycogen synthase kinase-3 (GSK-3) activity regulates mRNA methylation in mouse embryonic stem cells. *J. Biol. Chem.* **293**, 10731–10743
27. Soza-Ried, C., Bustamante, E., Caglevic, C., Rolfo, C., Sirera, R., and Marsiglia, H. (2019) Oncogenic role of arsenic exposure in lung cancer: A forgotten risk factor. *Crit. Rev. Oncol. Hematol.* **139**, 128–133
28. Wei, S., Zhang, H., and Tao, S. (2019) A review of arsenic exposure and lung cancer. *Toxicol. Res. (Camb.)* **8**, 319–327
29. Tam, L. M., Price, N. E., and Wang, Y. (2020) Molecular mechanisms of arsenic-induced disruption of DNA repair. *Chem. Res. Toxicol.* **33**, 709–726
30. Kanu, N., Cerone, M. A., Goh, G., Zalmas, L. P., Bartkova, J., Dietzen, M., McGranahan, N., Rogers, R., Law, E. K., Gromova, I., Kschischo, M., Walton, M. I., Rossanese, O. W., Bartek, J., Harris, R. S., *et al.* (2016) DNA replication stress mediates APOBEC3 family mutagenesis in breast cancer. *Genome Biol.* **17**, 185
31. Law, E. K., Sieuwerts, A. M., LaPara, K., Leonard, B., Starrett, G. J., Molan, A. M., Temiz, N. A., Vogel, R. I., Meijer-van Gelder, M. E., Sweep, F. C., Span, P. N., Foekens, J. A., Martens, J. W., Yee, D., and Harris, R. S. (2016) The DNA cytosine deaminase APOBEC3B promotes tamoxifen resistance in ER-positive breast cancer. *Sci. Adv.* **2**, e1601737
32. Huang, Y., Su, R., Sheng, Y., Dong, L., Dong, Z., Xu, H., Ni, T., Zhang, Z. S., Zhang, T., Li, C., Han, L., Zhu, Z., Lian, F., Wei, J., Deng, Q., *et al.* (2019) Small-molecule targeting of oncogenic FTO demethylase in acute myeloid leukemia. *Cancer Cell* **35**, 677–691.e10
33. Xu, Y., Zhang, W., Shen, F., Yang, X., Liu, H., Dai, S., Sun, X., Huang, J., and Guo, Q. (2021) YTH domain proteins: A family of m(6)A readers in cancer progression. *Front. Oncol.* **11**, 629560
34. Shi, H., Wei, J., and He, C. (2019) Where, when, and how: Context-dependent functions of RNA methylation writers, readers, and erasers. *Mol. Cell* **74**, 640–650
35. Li, J., Han, Y., Zhang, H., Qian, Z., Jia, W., Gao, Y., Zheng, H., and Li, B. (2019) The m6A demethylase FTO promotes the growth of lung cancer cells by regulating the m6A level of USP7 mRNA. *Biochem. Biophys. Res. Commun.* **512**, 479–485
36. Burns, M. B., Temiz, N. A., and Harris, R. S. (2013) Evidence for APOBEC3B mutagenesis in multiple human cancers. *Nat. Genet.* **45**, 977–983
37. Serebrenik, A. A., Argyris, P. P., Jarvis, M. C., Brown, W. L., Bazzaro, M., Vogel, R. I., Erickson, B. K., Lee, S. H., Goergen, K. M., Maurer, M. J., Heinzen, E. P., Oberg, A. L., Huang, Y., Hou, X., Weroha, S. J., *et al.* (2020) The DNA cytosine deaminase APOBEC3B is a molecular determinant of platinum responsiveness in clear cell ovarian cancer. *Clin. Cancer Res.* **26**, 3397–3407
38. Jomova, K., Jenisova, Z., Feszterova, M., Baros, S., Liska, J., Hudecova, D., Rhodes, C. J., and Valko, M. (2011) Arsenic: Toxicity, oxidative stress and human disease. *J. Appl. Toxicol.* **31**, 95–107
39. Kumagai, Y., and Sumi, D. (2007) Arsenic: Signal transduction, transcription factor, and biotransformation involved in cellular response and toxicity. *Annu. Rev. Pharmacol. Toxicol.* **47**, 243–262
40. Xiang, Y., Laurent, B., Hsu, C. H., Nachtergaele, S., Lu, Z., Sheng, W., Xu, C., Chen, H., Ouyang, J., Wang, S., Ling, D., Hsu, P. H., Zou, L., Jambhekar, A., He, C., *et al.* (2017) RNA m(6)A methylation regulates the ultraviolet-induced DNA damage response. *Nature* **543**, 573–576
41. Zhang, C., Chen, L., Peng, D., Jiang, A., He, Y., Zeng, Y., Xie, C., Zhou, H., Luo, X., Liu, H., Chen, L., Ren, J., Wang, W., and Zhao, Y. (2020) METTL3 and N6-methyladenosine promote homologous recombination-mediated repair of DSBs by modulating DNA-RNA hybrid accumulation. *Mol. Cell* **79**, 425–442.e7
42. Yu, F., Wei, J., Cui, X., Yu, C., Ni, W., Bungert, J., Wu, L., He, C., and Qian, Z. (2021) Post-translational modification of RNA m6A demethylase ALKBH5 regulates ROS-induced DNA damage response. *Nucleic Acids Res.* **49**, 5779–5797
43. Zhang, Q., Riddle, R. C., Yang, Q., Rosen, C. R., Guttridge, D. C., Dirckx, N., Faugere, M. C., Farber, C. R., and Clemens, T. L. (2019) The RNA demethylase FTO is required for maintenance of bone mass and functions to protect osteoblasts from genotoxic damage. *Proc. Natl. Acad. Sci. U. S. A.* **116**, 17980–17989
44. Cui, Y. H., Yang, S., Wei, J., Shea, C. R., Zhong, W., Wang, F., Shah, P., Kibriya, M. G., Cui, X., Ahsan, H., He, C., and He, Y. Y. (2021) Autophagy of the m(6)A mRNA demethylase FTO is impaired by low-level arsenic exposure to promote tumorigenesis. *Nat. Commun.* **12**, 2183
45. Huang, H., Weng, H., and Chen, J. (2020) m(6)A modification in coding and non-coding RNAs: Roles and therapeutic implications in cancer. *Cancer Cell* **37**, 270–288
46. Alarcon, C. R., Lee, H., Goodarzi, H., Halberg, N., and Tavazoie, S. F. (2015) N6-methyladenosine marks primary microRNAs for processing. *Nature* **519**, 482–485
47. Zhou, C., Molinie, B., Daneshvar, K., Pondick, J. V., Wang, J., Van Wittenberghe, N., Xing, Y., Giallourakis, C. C., and Mullen, A. C. (2017) Genome-wide maps of m6A circRNAs identify widespread and cell-type-specific methylation patterns that are distinct from mRNAs. *Cell Rep.* **20**, 2262–2276
48. Yi, Y. C., Chen, X. Y., Zhang, J., and Zhu, J. S. (2020) Novel insights into the interplay between m(6)A modification and noncoding RNAs in cancer. *Mol. Cancer* **19**, 121
49. Johnston, H. R., Keats, B. J. B., and Sherman, S. L. (2019) 12 - population genetics. In: Pyeritz, R. E., Korf, B. R., Grody, W. W., eds. *Emery and Rimoin's Principles and Practice of Medical Genetics and Genomics*, 7th Ed, Academic Press, San Diego, CA: 359–373
50. Tubbs, A., and Nussenzweig, A. (2017) Endogenous DNA damage as a source of genomic instability in cancer. *Cell* **168**, 644–656
51. Ackerman, S., and Horton, W. (2018) Chapter 2.4 - effects of environmental factors on DNA: Damage and mutations. In: Török, B., Dransfield, T., eds. *Green Chemistry*, Elsevier, Cambridge, MA: 109–128
52. McInerney, P., Adams, P., and Hadi, M. Z. (2014) Error rate comparison during polymerase chain reaction by DNA polymerase. *Mol. Biol. Int.* **2014**, 287430
53. Gao, M., Chen, M., Li, C., Xu, M., Liu, Y., Cong, M., Sang, N., and Liu, S. (2018) Long non-coding RNA MT1DP shunts the cellular defense to cytotoxicity through crosstalk with MT1H and RhoC in cadmium stress. *Cell Discov.* **4**, 5